

# Semi-analytical dark matter halos and the Jeans equation

Crystal G. Austin, Liliya L.R. Williams, Eric I. Barnes

*Astronomy Department, University of Minnesota, Minneapolis, MN 55455*

`caustin, llrw, barnes@astro.umn.edu`

Arif Babul<sup>1</sup>

*Department of Physics and Astronomy, University of Victoria, BC, Canada*

`babul@uvic.ca`

Julianne J. Dalcanton<sup>2</sup>

*Astronomy Department, University of Washington, Box 351580, Seattle, WA 98195*

`jd@astro.washington.edu`

## ABSTRACT

Although N-body studies of dark matter halos show that the density profiles,  $\rho(r)$ , are not simple power-laws, the quantity  $\rho/\sigma^3$ , where  $\sigma(r)$  is the velocity dispersion, is in fact a featureless power-law over  $\sim 3$  decades in radius. Here, we demonstrate that this property is common to halos whose collapse and formation is modeled fully with numerical or semi-analytic techniques. Using the Extended Secondary Infall Model (ESIM), we demonstrate that the nearly scale-free nature of  $\rho/\sigma^3$  is a robust feature of virialized halos in equilibrium and one must concoct rather extreme conditions to cause significant deviations from a simple power-law. At present, there are no detailed studies that provide a physical explanation for this behavior. By examining the processes in common between numerical and semi-analytic approaches, we argue that the scale-free nature of  $\rho/\sigma^3$  cannot be the result of hierarchical merging, rather it must be an outcome of violent relaxation. An analytic analysis shows that while the Jeans equation of hydrostatic equilibrium does not isolate a unique value of the power-law index ( $\rho/\sigma^3 \propto r^{-\alpha}$ ), it does point to  $\alpha = 1.9444$  as a special solution.

*Subject headings:* Dark Matter

---

<sup>1</sup>Leverhulme Visiting Professor, Universities of Oxford and Durham

<sup>2</sup>Alfred P. Sloan Research Fellow

## 1. Introduction

There is a broad consensus that gravity-driven cosmological evolution of collisionless cold dark matter, starting from some realistic matter power spectrum, results in virialized objects whose spherically-averaged density profile is well represented by the NFW prescription (Navarro et al. 1997), or its close variants (Moore et al. 1998; Navarro et al. 2004). The main characteristics of the density profile are the relatively shallow density slope in the center,  $d \log \rho / d \log r \sim -1$ , and much steeper slope around the virial radius,  $\approx -3$ . These general properties are well established, but the details are not. The value of the central slope, and the nature of the transition between inner and outer slopes is still a matter of debate. Currently, some advocate the original NFW formulation with constant asymptotic density slopes and a scale-radius (Diemand et al. 2005). Others argue for a more continuous change of the slope as a function of radius (Navarro et al. 2004; Merritt et al. 2005). Regardless of which density profile expression proves to best describe N-body halos, the underlying physics that drives the halos to have this shape is not yet fully understood.

Several attempts have been made in the literature to explain the density profile shape. For example, Syer & White (1998) suggested that the NFW profile results from a series of repeated mergers; as the undigested cores of merging satellites accumulate at the center, the central  $r^{-1}$  cusp develops. However, Huss et al. (1999) performed simulations of isolated halos with varying degrees of thermal motion of dark matter particles. The final halos closely resembled the universal NFW shape, suggesting that hierarchical merging is not critical to the outcome. Moore et al. (1999) simulated halo formation using a matter power spectrum with suppressed small scale power. The final density profiles were still well described by the NFW fit. Some analytical studies suggest that secondary infall and accretion can determine the density profile shape (Avila-Rees et al. 1998). Barnes et al. (2005a) argue that the density profile, and in particular its radially changing slope, is the result of a mild aspect of the radial orbit instability.

A different approach was taken by Taylor & Navarro (2001) (hereafter TN01), and Hansen (2004). Instead of considering the radial run of the space density of N-body halos, they measured the quantity  $\rho(r)/\sigma^3(r)$ , which has the dimensionality of phase-space density. In spherically-symmetric equilibrium halos,  $\rho/\sigma^3$  is proportional to the coarse-grained phase-space density, a quantity distinct from the (fine-grained) phase-space density whose conservation is ensured by the collisionless Boltzmann equation (*e.g.* Dehnen 2005). As our analysis does not hinge on the strict interpretation of the quantity  $\rho/\sigma^3$ , we will continue to call it phase-space density, for brevity.

TN01 found that  $\rho/\sigma^3$  of their three halos (circular velocities 160-200 km s<sup>-1</sup>) is very well approximated by a single power-law, from  $10^{-2.5}$  virial radii to just beyond the virial radius. This finding is unexpected because the density profile,  $\rho(r)$  undergoes a considerable slope change in the same radial interval. The scale-free nature of the phase-space density

implies that the double logarithmic slope of the velocity dispersion changes in such a way so as to offset the change in the density profile slope. The power-law index  $\alpha$ , where  $\rho/\sigma^3 \propto r^{-\alpha}$ , was found to be very similar for all the three halos studied by TN01;  $\alpha = 1.875$ .

Does the power-law nature of  $\rho/\sigma^3$  characterize all equilibrium N-body halos, or are the halos studied by TN01 somehow special? One can get a rough answer to this question without analyzing many individual simulation halos. Given the form of a “universal” empirical fit to N-body halos and assuming that the halos are in equilibrium, one can calculate the phase-space density as a function of radius using the Jeans equation. Barnes et al. (2005b) use two types of empirical fits to N-body profiles (Navarro et al. 1997, 2004) to demonstrate that both produce nearly scale-free phase-space density profiles for  $\sim 3$  decades in radius, with a slope close to 1.9. They conclude that most N-body halos should have scale-free phase-space density profiles. This conclusion is further supported by a recent study of equilibrium halos (Kazantzidis et al. 2004). The halo that most resembles results of N-body simulations has scale-free  $\rho/\sigma^3$  and index  $\alpha \approx 1.95$ .

The scale-free nature of  $\rho/\sigma^3$  represents a novel way of looking at the properties of halos, and as such, should be explored further. If this property is “universal”, it amounts to a hitherto unrecognized constraint on the shape of the density profiles. In this paper we address questions related to the  $\rho/\sigma^3$  profiles of collisionless halos. Is the scale-free nature of  $\rho/\sigma^3$  (i) a result of initial conditions, (ii) an outcome of evolution and virialization, or (iii) a consequence of the final equilibrium state of halos? In a related work, Barnes et al. (2005b) address the third question. They demonstrate that the condition of hydrostatic equilibrium alone, as quantified by the Jeans equation, does not require  $\rho/\sigma^3$  to be a power-law in radius.

The first two questions can be addressed by studying halo formation techniques different from N-body simulations. Semi-analytical methods based on the secondary infall paradigm are an example of such techniques. Halos forming in N-body simulations are subject to a complex set of dynamical processes. Particles can exchange energy and momentum through violent relaxation and two-body encounters (even though the latter are suppressed in cosmological simulations). Additionally, phase-mixing can decrease phase-space density, while preserving particles’ energies. These processes are brought about by halo collapse, merging, dynamical friction, etc. The analytical methods do not incorporate such a wide range of processes. The method we use here is based on Ryden & Gunn (1987), and was extended by Williams et al. (2004); we call it ESIM, the Extended Secondary Infall Model. As we describe later in more detail, ESIM halos are spherically symmetric with one spatial and two velocity (radial and tangential) phase-space dimensions. They virialize through violent relaxation, which changes the shells’ energies, but conserves the angular and radial momenta of each shell throughout the collapse. There are no mergers.

Given such different formation scenarios, it is not surprising that the final properties—density distributions, etc.—of N-body and ESIM halos tend to be different. (See Barnes

et al. (2005a) for a discussion of why the two types of density profiles differ.) However, if specific final properties are present in N-body and ESIM halos, that strongly suggests that the property is the result of shared physics. This is our premise in addressing question (ii). Specifically, we find that the phase-space density of our halos is well represented by a power-law (Section 2), a result similar to the one reached through the study of numerically generated halos. Question (i) is also addressed in Section 2, where we vary input conditions of ESIM halos. Again, the power-law nature of  $\rho/\sigma^3$  does not seem to be affected by these indicating that the answer to question (i) is negative.

In Sections 3 we address the behavior of index  $\alpha$ . One of the main properties of the virialized halos is that they are in equilibrium, so the Jeans equation is important in determining the structure of halos. Therefore it makes sense to ask if the Jeans equation has a preferred value for  $\alpha$ , or, if all values are equally likely from the point of view of the Jeans equation. Our analysis of the second derivative of the Jeans equation and its various solutions leads to some interesting insights (also see Appendix A). Appendix B derives the value of  $\alpha$  for halos formed in a highly idealized secondary infall model (SIM), and compares it to  $\alpha$ 's obtained in ESIM halos of Section 2.

## 2. Extended Secondary Infall Model (ESIM) Halos

### 2.1. Summary of the Method

The collisionless dark matter halos in the present study are formed using an analytical method originally introduced by Ryden & Gunn (1987). The method, including minor extensions, is fully described in Williams et al. (2004); we summarize it briefly. Halos are spherically symmetric and isolated. The density profile of a proto-halo is taken to be the profile of a peak in a density field described by standard CDM power spectrum,  $P(k)$  (Bardeen et al. 1986). In addition to the primary peak, proto-halos have superimposed secondary perturbations, whose properties are derived from the same  $P(k)$ . In a real halo these secondary perturbations generate random motions of dark matter particles, both radial and tangential. In ESIM halos the RMS amplitude of random velocities (as a function of radius) are calculated from  $P(k)$ , as described in Ryden & Gunn (1987). For each shell the magnitude of the velocity perturbation is chosen from a Maxwell-Boltzmann distribution with the above RMS; the direction is chosen randomly.

When a particular shell reaches its maximum turn-around radius the perturbation in radial and tangential velocity is added to the existing radial infall velocity. In a real halo these additional random velocities result in dark matter particles having elliptical, precessing orbits. In ESIM halos, the random velocities transform the initially thin shells into thick, overlapping shells, each with its own apo- and peri-center. A key assumption in ESIM calculations is that the collapse proceeds adiabatically, with each shell conserving its angular

and radial momentum. Note that each shell’s secondary perturbation momentum is oriented randomly, so that the halo as a whole has zero net angular momentum, and no net rotation. As the collapse proceeds, the mass distribution in the halo changes, and the potential and shells’ energies are recalculated after each step in the collapse. This is violent relaxation. To sum up, ESIM halos are formed via smooth accretion of somewhat lumpy material, with no major mergers.

Our method of halo formation has considerable flexibility with direct control over the parameter space of initial conditions. For example, we can change the shape of the primary density peak by smoothing or altering the matter power spectrum. Both the shape of the primary peak and the amplitude of the secondary perturbations are based on  $P(k)$ , but we can alter the shape of the primary peak and the amplitude of secondary perturbations independently, which gives us another degree of freedom in exploring the parameter space of halos. For example, we can change the secondary perturbations—the overall amplitude and radial dependence—while keeping the primary peak unaltered. Even though these changes need not correspond to any astrophysically plausible scenarios the evolution of ESIM halos proceeds in a physically consistent way.

## 2.2. ESIM Halo Calculation Results

We generate three sets of halos, with ‘galaxy’, ‘group’ and ‘cluster’ scale masses. To get different ranges of halos mass we filter the mass power spectrum, prior to normalization, on comoving scales  $r_h$  of 0.05, 0.35 and 0.7 Mpc, respectively. Larger  $r_h$  mean that the collapse will start later, and more massive halos will form as a result. Within each mass set we study the effect of the secondary velocity perturbations on the final halo profiles. To that end, we form halos where the magnitudes of the secondary velocity perturbations are scaled by a parameter, hereafter called the perturbation amplitude scaling parameter, or scaling parameter for short. In this Section the scaling parameter is altered uniformly for a given halo, but in Section 2.3 we radially vary it within the halos. A scaling parameter of zero corresponds to no secondary perturbations, in which case the velocities are purely radial. A scaling parameter of 1 corresponds to the original amplitude of secondary perturbations derived from the same power spectrum that determined the shape of the primary density peak, while setting the scaling parameter to 2 doubles the amplitude of all secondary perturbations.

The perturbation amplitude scaling parameter is varied from 0.4 to 2.5 in increments of 0.05. Because each shell is assigned a velocity perturbation from a distribution extending to  $\approx 2.5V_{rms}$ , there is a chance that the shell’s kinetic energy will exceed its potential energy. This is especially likely if the scaling parameter is large, and the shell happens to be far from center. In this case, we assume that the shell is instantaneously lost from the halo and is no longer considered in the potential calculations or the kinematic analysis. Each

shell's potential energy is calculated based on the mass distribution due to a finite number of shells, with the outermost shells extending well beyond the virialized portion of the halo at the present epoch. The total number of shells, and hence the zero-point of the potential, is fixed such that halos computed using scaling parameters less than 1.5 do not lose any mass during the collapse, while halos with a scaling parameter of 2 lose at most 25% of their final mass.

Each ESIM halo is unique since the secondary velocities for each shell are picked randomly from a distribution. To reduce the dispersion in the final halo properties the halos presented here are averages of ten individual halos. To verify the reliability of the results two sets of averaged halos were computed for each scaling parameter. In all cases our analysis applies to the portion of each halo between  $10^{-2.5}$  and 1 virial radius,  $r_{200}$ , the radius at which the average enclosed halo density is 200 times the critical,  $\rho_o = 2.77 \times 10^{11} h^2 M_\odot \text{ Mpc}^{-3}$ .

In the following sections we describe the various properties of the final virialized ESIM halos. In Sections 2.2.1-2.2.4 we discuss in detail the properties of galaxy mass halos. Since the qualitative properties and the general trends are similar for galaxy, group, and cluster mass halos, we do not discuss the latter two specifically, but present a summary of their properties in Section 2.2.5.

Throughout this paper we assume standard CDM model with matter-dominated flat geometry, and matter power spectrum  $P(k)$  normalized such that  $\Omega^{0.6} \sigma_8 = 0.5$  and  $h = 0.5$ . Our assumed cosmological parameters are not the currently favored ones, however, this fact has a minimal effect on the final halo properties of interest.

### 2.2.1. Density profiles

Figure 2.2.1 shows four halo density profiles, in units of critical density  $\rho_o$ , and multiplied by  $(r/r_{200})^2$  to accentuate features in the density profiles. All were generated using the galaxy-mass  $P(k)$  filtering scale  $r_h = 0.05 \text{ Mpc}$ . The standard case, a halo with a scaling parameter of 1, is shown in panel C. Panels A, B and D show halos with scaling parameter of 0.4, 0.6 and 2, respectively.

As in Williams et al. (2004), the ESIM halos differ from those in N-body simulations. For convenience, NFW density profiles,  $\rho(r) \propto (r/r_s)(1 + r/r_s)^2$  (Navarro et al. 1997), with concentration parameter ( $c = r_{200}/r_s$ ) appropriate for that halo mass, and arbitrary normalization are over-plotted as long dash lines. Unlike NFW profiles, ESIM density profiles are well approximated by a single power-law between  $r = 10^{-2.5} r_{200}$  and  $r_{200}$ .

The effects of changing the amplitude of secondary perturbations on the mass distribution in the halos can be seen in the four panels of Figure 2.2.1, and is summarized in panel A of Figure 2.2.1, which plots  $\gamma_{fit}$ , the fitted density profile slopes, vs. scaling param-

eter. As expected, the halos with larger secondary perturbations, and hence more angular momentum have shallower density profiles. To further characterize the density profiles we indicate in Figure 2.2.1 where the slope,  $\gamma = -(d \ln \rho)/(d \ln r)$ , attains the values of  $\gamma=1$ , 2, and 3, with dotted, short-dash and long dash lines. We denote these radii by  $r_{\gamma=1}$ ,  $r_{\gamma=2}$ , and  $r_{\gamma=3}$ . The dependence of  $r_{\gamma=1,2,3}$  with respect to the scaling parameter is shown in panel D of Figure 2.2.1. The values of  $r_{\gamma=1,2,3}$  increase with the scaling parameter, consistent with density profiles becoming shallower as the angular momentum content of the halos increase.

### 2.2.2. Velocity dispersion and velocity anisotropy

Since many shells overlap at any given radius, the total velocity dispersion profile is calculated as the mass-weighted and time-weighted RMS value of the radial and tangential velocity dispersions of all the shells that exist at that radius. Figure 2.2.2 shows the velocity dispersion profiles for the halos presented in Figure 2.2.1. The values of  $r_{\gamma=1}$ ,  $r_{\gamma=2}$ , and  $r_{\gamma=3}$  are marked as dotted, short-dash and long-dash lines. Figure 2.2.2 also shows the velocity dispersion anisotropy,  $\beta$ , defined as usual, through the radial and tangential velocity dispersions (Binney & Tremaine 1987),

$$\beta \equiv 1 - \frac{\sigma_\theta^2}{\sigma_r^2} \quad (1)$$

Except for halos generated using small scaling parameter values,  $\lesssim 1$ , the anisotropy parameter stays close to 0 between  $\sim 10^{-3}$  and  $\sim 1$  virial radii. For the standard halo, the average velocity anisotropy parameter is  $\beta \sim 0.1$ . Beyond the virial radius, the velocity ellipsoid parameter increases to  $0.5 - 1$  as the orbits become more radial. In general, a halo's average  $\beta$  increases with decreasing scaling parameter: smaller secondary perturbations imply less angular momentum, and hence more radial orbits. In the limit of perturbation amplitude scaling parameter of 0, purely radial orbits will result.

### 2.2.3. Phase-space density

The phase-space density profiles of the halos displayed in Figure 2.2.1 are shown in Figure 2.2.3. It is apparent that ESIM halos have nearly scale-free distribution of  $\rho/\sigma^3$  extending over 2–4 decades in radius. This figure demonstrates that the scale-free nature of  $\rho/\sigma^3$  is resilient: it persists despite the uniform changes in the magnitude of the secondary perturbations. However, the power-law index,  $\alpha = -(d \ln \rho/\sigma^3)/(d \ln r)$ , is not constant; in general,  $\alpha_{fit}$  increases with increasing scaling parameter (see panel B of Figure 2.2.1).

#### 2.2.4. Halo mass

Panel C of Figure 2.2.1 shows that the mass of virialized halos, for a given power spectrum filtering length ( $r_h = 0.05\text{Mpc}$  for these halos), decreases steadily as the perturbation amplitude scaling parameter increases. Large secondary perturbation amplitude implies a more extended mass distribution, and smaller virial masses. Additionally, if the shells' energy reaches the threshold to cause mass loss, the final mass is reduced further. However, this effect is negligible for most halos: there is no mass loss during formation for halos with the scaling parameter less than about 1.5-2.

#### 2.2.5. ESIM halos of galaxy, groups and cluster masses.

So far, we have discussed how the properties of galaxy-mass halos ( $r_h = 0.05\text{Mpc}$ ) change with the changing amplitude of secondary perturbations. Group and cluster-mass halos, generated using power spectrum filtering lengths of  $r_h = 0.35$  and  $0.7\text{Mpc}$ , respectively, behave similarly. The overall trends are summarized in Figures 2.2.5 and 2.2.5, which are similar to Figure 2.2.1. Two examples of the shapes of density and phase-space density profiles are shown in Figure 2.2.5, for  $r_h = 0.35\text{Mpc}$  (panels A and C) and  $r_h = 0.7\text{Mpc}$  (panels B and D); both halos have scaling parameter of 1. It is apparent that larger  $r_h$  values result in density profiles that are not as well described by a single power-law, as smaller  $r_h$  halos. This is further illustrated in panels D of Figure 2.2.5 and 2.2.5;  $r_{\gamma=1}$ ,  $r_{\gamma=2}$  and  $r_{\gamma=3}$  are closer together than in galaxy-mass halos, implying that the density slope changes more rapidly with radius.

Despite the non power-law behavior of density, the phase-space density,  $\rho/\sigma^3$  remains a power-law for at least 2-3 decades in radius interior to  $r_{200}$  (panels C and D of Figure 2.2.5). The best-fit slope  $\alpha_{fit}$  increases with the scaling parameter for a fixed  $r_h$  (panels B of Figure 2.2.1-2.2.5), but gets consistently smaller with increasing  $r_h$ .

Figure 2.2.5 depicts the dependence of the  $\rho/\sigma^3$  power-law slope,  $\alpha_{fit}$  on the virial mass for all three sets of halos:  $r_h = 0.05$  Mpc (triangles),  $r_h = 0.35$  Mpc (squares), and  $r_h = 0.7$  Mpc (pentagons). Filled symbols show  $\alpha_{fit}$  obtained by fitting a power-law to the data within our standard radial range, from  $10^{-2.5}$  to 1 virial radii. To test the dependence of the specific choice of the radial range we also use a reduced range of  $10^{-2.5}$  to  $10^{-0.5}$  virial radii (empty symbols). The  $\alpha_{fit}$  values are similar in both cases. The main conclusion from Figure 2.2.5 is that  $\alpha_{fit}$  is not uniquely determined by any single property of halos that we can control, such as mass, perturbation amplitude scaling parameter, or  $r_h$ .

### 2.3. Testing the Resiliency of the $\rho/\sigma^3$ Power-law

Since the halos considered in previous sections exhibit a near-perfect power-law in  $\rho/\sigma^3$ , we wish to determine what would be required to break this resilient behavior. To that end, we generate halos with different scaling parameters assigned to blocks of shells. These changes are not meant to mimic realistic situations, but rather to push our simulations to unphysical extremes. In several trials we increased or decreased the scaling parameter linearly with radius; in other trials, we assigned the inner 5-15% of radii a larger perturbation amplitude scaling parameter of 5, 20, or 50, with smaller scaling parameters assigned to outer shells.

The halos with the scaling parameter assigned linearly in radius (with no large discontinuities) display the power-law in  $\rho/\sigma^3$ . However, halos in the trials with the ‘excited sections’ (blocks of shells with large scaling parameters) had a  $\rho/\sigma^3$  profile that showed deviations from a power-law behavior. Figure 2.3 shows the specific halo where all the shells were assigned a scaling parameter of 0.9, except for those with an initial comoving radius between 0.59 and 0.79 Mpc, which were assigned a scaling parameter of 5. The last shell to collapse in this evolution had a comoving radius of 1.92 Mpc. Visual inspection of panels A and B show that, even though these halos have been subjected to radially discontinuous changes in the amplitude of the secondary perturbations, the final density and velocity dispersion profiles still track each other rather well. As a consequence, the combination  $\rho/\sigma^3$  still resembles a power-law, but the deviations are evident. This and other similar trials illustrate that one must adopt extreme measures—large discontinuities in the scaling parameter—in order to break the scale-free nature of the phase-space density profile.

### 2.4. Conclusions from ESIM Halos

The ESIM formalism provides us with a simplified, but physically correct way of generating collisionless dark matter halos. It is very different from N-body simulations. In the preceding sections we described ESIM halo properties in detail, pointing out that the density profiles are generally different from those produced in N-body simulations. By changing the initial conditions we produced a range of density profile types: by filtering the mass power spectrum on small scales ( $r_h = 0.05$ Mpc) to simulate galaxy-mass halo formation, we ended up with density profiles that showed virtually no change in slope over 2-3 decades in radius inside of the virial radius (Figure 2.2.1). Larger filtering scales ( $r_h = 0.35$  and 0.7 Mpc) aimed to produce group and cluster-mass halos resulted in more curved density profiles (Figure 2.2.5).

The most important conclusion of Section 2 concerns the phase-space density profile,  $\rho/\sigma^3$ . Despite the differences in methods and density profile shapes, one feature was shared by all ESIM halos and N-body simulated halos: the power-law nature of the  $\rho/\sigma^3$  profile. We have shown that this feature of ESIM halos is very resilient, and one must concoct rather

extreme cases in order to end up with  $\rho/\sigma^3$  that shows deviations from a single power-law (Section 2.3). There are no models in astrophysics literature that provide a physical explanation for this feature of virialized halos. We argue that the scale-free nature  $\rho/\sigma^3$  cannot be uniquely characteristic of hierarchical merging because ESIM halos do not undergo mergers. We speculate that it is a generic consequence of the one dynamical process which is common to both ESIM and N-body halo formation—violent relaxation, or, global changes in the potential, and the accompanying changes in particle energies brought about by the collapse.

Our results concerning  $\alpha$ , the double logarithmic slope of  $\rho/\sigma^3$  vs. radius, are different from those of TN01. We find a range of values from 1.6 to 2.2, while TN01 find that the same  $\alpha = 1.875$  described all three of their N-body halos. It is possible that the latter finding is due to a small number of halos studied. In our study,  $\alpha$  was not uniquely determined by any single property of halos, such as mass, epoch of formation, or amplitude of random velocities.

### 3. Jeans equation analysis

#### 3.1. The second derivative of the Jeans equation

The findings of the preceding section, summarized in Section 2.4, motivate our next step. ESIM halos are spherically symmetric, in equilibrium, have zero net angular momentum, and have approximately isotropic velocity dispersion ellipsoids,  $\beta \approx 0$ .<sup>1</sup> These halo properties lead directly to the appropriate version of the Jeans equation, and its first derivative:

$$\frac{d(\rho\sigma^2)}{dr} = -\rho \frac{GM(< r)}{r^2}, \quad (2)$$

which states that halos are supported against collapse by “pressure,” provided by the velocity dispersion of dark matter particles. In Section 2 we have established empirically that ESIM halos exhibit scale-free  $\rho/\sigma^3$  behavior. In this paper we will not address the question of *why* phase-space density radial profiles are power-laws. Instead, we will take this property as an additional constraint:

$$\frac{\rho}{\sigma^3}(r) = \frac{\rho_0}{\sigma_0^3} \left(\frac{r}{r_0}\right)^{-\alpha}. \quad (3)$$

where  $\rho_0$ ,  $r_0$ ,  $\sigma_0$ , and  $\alpha$  are constants for any given halo. Eliminating  $\sigma$ , and using the dimensionless variables,  $x = r/r_0$  and  $y = \rho/\rho_0$ , we can now write down the derivative of equation 2,

$$\frac{d}{dx} \left[ \frac{-x^2}{y} \frac{d}{dx} (y^{5/3} x^{2\alpha/3}) \right] = \kappa y x^2. \quad (4)$$

---

<sup>1</sup>Looking at Figure 2.2.2 zero anisotropy is arguably the least justified of our assumptions, and we will relax it in the next paper. As a place to start,  $\beta \approx 0$  is a reasonable approximation.

This is also equation 4 of TN01. The constant  $\kappa = 4\pi G\rho_0 r_0^2/\sigma_0^2$  specifies the normalization of halos. Exponent  $\alpha$  is constant for any given halo, but we leave its value unspecified.

In the rest of this Section we develop a framework for studying halos that can be described by equation 4. However, unlike the earlier Jeans equation work our main equation will not be equation 4 itself, but its first derivative, which is also the second derivative of the Jeans equation:

$$(2\alpha + \gamma - 6)(2\alpha - 5\gamma)(\frac{2}{3}[\alpha - \gamma] + 1) = 3\gamma'(8\alpha - 5\gamma - 5) + 15\gamma'', \quad (5)$$

where we have defined logarithmic derivatives of the density slope,  $\gamma = -d \ln y / d \ln x$ , as  $\gamma' = d\gamma/d \ln x$ , and  $\gamma'' = d\gamma'/d \ln x$ . Equation 5 has several advantages over equation 4. It does not depend on the normalization constant  $\kappa$ , and has no explicit dependence on  $x$ , in fact, equation 5 depends only on the exponent  $\alpha$ , and the local density slope,  $\gamma(x)$ . Equation 5 looks like an algebraic equation—its partially factorized form will prove useful in exploring the various types of solutions of the Jeans equation.

Our goal in the following is to explore solutions of the Jeans equation in general, paying particular attention to the role of  $\alpha$ . Specifically, we want to know if the Jeans equation admits any special  $\alpha$  values.

### 3.2. The $\alpha - \gamma$ plane

A halo is characterized by a relation between  $\gamma$  and  $x$ , which can be obtained by assuming a value for  $\alpha$ , specifying initial conditions for  $\gamma$  and  $\gamma'$ , and then integrating equation 5. An infinite variety of halos can be generated in this fashion, so a straightforward exploration of the parameter space is probably not the most insightful one. The form of equation 5, namely that it looks like a factorized algebraic equation of two variables,  $\alpha$  and  $\gamma$ , suggests that it is instructive to consider the  $\alpha - \gamma$  plane, shown in Figure 3.2. Assuming  $\alpha$  is constant for any given halo, a halo density profile can be represented by a vertical straight line segment.

There are four factors in equation 5, three on the LHS, and one on the RHS. By separately setting these to zero we obtain the four thick lines in the  $\alpha - \gamma$  plane. This plot provides a framework for understanding and classifying different types of solutions of the Jeans equation.

Consider the line  $2\alpha - 5\gamma = 0$  (lower thick solid line). If part of a halo is described by a constant  $\gamma = (2/5)\alpha$  for some range of radii, then the LHS of equation 2 can be expressed as  $d \ln(\rho\sigma^2) / d \ln r \propto 2\alpha - 5\gamma$ , implying that the pressure gradient vanishes in that part of the halo. An example of this is the central region of the critical solution identified by TN01, where  $\gamma = 0.75$ , corresponding to  $\alpha = 1.875$ . In general, halos of any  $\alpha$  whose inner profile slope is described by  $2\alpha - 5\gamma = 0$  have vanishing pressure gradient in the center.

The role of terms  $2\alpha + \gamma - 6$  and  $8\alpha - 5\gamma - 5$  is addressed in Sections 3.3 and 3.4 respectively. The term  $\frac{2}{3}[\alpha - \gamma] + 1$  is briefly discussed in Section A, and all four terms of equation 5 are important in the discussion of Section 3.4.

### 3.3. Power-law density profiles

One of the factors on the LHS of equation 5 is  $2\alpha + \gamma - 6$ ;  $2\alpha + \gamma - 6 = 0$  is shown as the long-dash line in Figure 3.2.  $\gamma_{pl} = 6 - 2\alpha$  represent power-law density profile solutions to the Jeans equation (TN01, Hansen (2004)), i.e. if  $\gamma' = \gamma'' = 0$  then  $\gamma_{pl} = \text{const}$  for all  $x$ . A power-law density profile is represented by a point in Figure 3.2. For example, the singular Isothermal Sphere is a viable solution of equation 5, characterized by  $\alpha = \gamma = 2$  and constant  $\sigma$  throughout the halo.

Because equation 5 does not distinguish between the three factors on the LHS, one might think that each of these three should produce power-law density profiles. This is not so. Equation 4 can be rewritten as  $(2\alpha - 5\gamma)(\frac{2}{3}[\alpha - \gamma] + 1) - 5\gamma' = -3\kappa x^{2-\frac{2}{3}\alpha} y^{1/3}$ . If the slope  $\gamma$  is given by  $2\alpha - 5\gamma = 0$ , or  $\frac{2}{3}[\alpha - \gamma] + 1 = 0$ , and  $\gamma' = 0$  because we are dealing with a power-law density profile, then the RHS becomes zero, which is unphysical. (Recall that  $y$  is scaled density.) Therefore, for a given  $\alpha$  there is a unique power-law density solution,  $\gamma_{pl} = 6 - 2\alpha$ .

The one-to-one correspondence between  $\gamma_{pl}$  and  $\alpha$  can be tested using ESIM halos. Galaxy-mass ( $r_h = 0.05$  Mpc) ESIM halos presented in Section 2.2 have nearly power-law density profiles. Of these, halos with the perturbation amplitude scaling parameters of 1 or larger have nearly isotropic velocity dispersion ellipsoids. For these halos the relation between the fitted slopes of the density and phase-space density profiles should follow  $2\alpha_{fit} + \gamma_{fit} - 6 = 0$ . In Figure 3.2 we plot  $\alpha_{fit}$  and  $\gamma_{fit}$  for halos with scaling parameters between 1 and 2.5 (crosses). There is good agreement between ESIM halo data and predictions.

### 3.4. The unique periodic solution of Equation 5

Equation 5 is a non-linear damped oscillator equation for  $\gamma$ , with the  $\gamma'$  term being analogous to a dissipation term. Equation 5 therefore suggests that the Jean's equation may admit solutions where the slope of the density profile oscillates with radius, becoming alternately steeper and shallower. If equation 5 is in a regime where these oscillations are damped, then the slope  $\gamma$  may oscillate, with the amplitude of the oscillations decaying with increasing radii. Asymptotically, this behavior would lead to a density profile that has a power-law fall-off at large radii. Instead, if equation 5 is in a regime where the oscillations can amplify, then the slope may run away to large values, leading to a density profile that

becomes increasingly steep at large radii.

The coefficient of the  $\gamma'$  term in equation 5 controls the “dissipation” in the oscillations of the density profile slope  $\gamma$ . If this coefficient were always positive (negative), it would damp (amplify) the amplitude of  $\gamma$  oscillations with  $\ln x$ .<sup>2</sup> If the coefficient is zero, the amplitude of oscillations would not evolve, resulting in perpetually periodic oscillations. In the case of equation 5, the damping term is non-linear, with its sign changing as a function of  $\ln x$ . Does a periodic solution exist in such a situation?

Let us use Figure 3.2 as a guide. Notice that the point of intersection of  $8\alpha - 5\gamma - 5 = 0$  and  $2\alpha + \gamma - 6 = 0$  lines is exactly half-way between  $2\alpha - 5\gamma = 0$  and  $\frac{2}{3}[\alpha - \gamma] + 1 = 0$ . The corresponding  $\alpha = 35/18 = 1.9444$ , and with that equation 5 can be rewritten as

$$\gamma'' = \frac{2}{9}B\left(\left[\frac{4}{3}\right]^2 - B^2 - \frac{9}{2}\gamma'\right), \quad (6)$$

where  $B = \gamma_{pl} - \gamma$ , and  $\gamma_{pl} = 2.111$  for  $\alpha = 1.9444$ . Equation 6 says that when  $B = 0$ , then  $\gamma'' = 0$ , and hence  $\gamma'$  attains a local minimum or maximum. So, every time  $\gamma = 2.111$ ,  $\gamma'$  attains an extremum. This statement can be true only if  $\gamma$  varies periodically with  $\ln x$ . Getting back to the coefficient of the damping term: when  $\alpha = 1.9444$ , the value of  $8\alpha - 5\gamma - 5$  is, on average, zero.

Thus,  $\alpha = 1.9444$  results in periodic solutions, and Figure 3.2 tells us that this  $\alpha$  value is unique. The amplitude of the wave, i.e. the minimum and maximum values of  $\gamma$ , and its period of oscillations, i.e. the radial span in the halo between steepest and shallowest slopes, depend on the initial conditions. The maximum amplitude is attained for initial  $\gamma' = 0$ , and initial  $\gamma$  somewhat larger than  $(2/5)\alpha$  (lower thick solid line in Figure 3.2), or somewhat smaller than  $\alpha + 1.5$  (upper thick solid line in Figure 3.2). As the initial  $\gamma$  is set closer to  $\gamma_{pl} = 6 - 2\alpha = 19/9 \approx 2.111$  the amplitude of oscillations decreases. For the exact  $\gamma_{pl}$  we get a power-law density profile, as already noted in Section 3.3. The periodic behavior is illustrated in Figure 3.4 which shows the limit cycle of equation 5, as long-dash and dotted line closed curves. For both of these  $\alpha = 1.9444$  and initial  $\gamma' = 0$ , but initial  $\gamma_{in}$ 's are different (0.7788 and 2.7111).

The shape of the upper portion of the  $\alpha = 1.9444$ ,  $\gamma_{in} \approx (2/5)\alpha$  ( $=0.7788$ ) curve in Figure 3.4 (long-dash line) suggests that the corresponding solution of the Jeans equation has a simple analytical form—a parabola. In fact, equation 5 does admit the following solution:

$$\gamma' = \gamma'_m - \frac{1}{6}(\gamma - \gamma_0)^2, \quad \gamma_0 = \frac{1}{15}(55 - 12\alpha), \quad \gamma'_m = \frac{\gamma_0^2}{6} + \frac{2\alpha(\alpha - 3)(2\alpha + 3)}{5(6\alpha + 1)}. \quad (7)$$

---

<sup>2</sup>We stress that the halos are in equilibrium, and the use of the word “oscillations” does not mean that the halos are changing in time: the changes are in the density profile slope, as a function of logarithmic radius.

Equations 7 allow us to express the density profile slope as a function of radius in the halo:

$$\gamma = (6\gamma'_m)^{1/2} \tanh [(\gamma'_m/6)^{1/2} \ln x] + \gamma_0. \quad (8)$$

This solution is valid exactly only for the halo with  $\alpha = 1.9444$  and asymptotic density slopes,  $\gamma_{in} = 0.7778$  and  $\gamma_{out} = 3.444$ , given by the intersection of the  $\alpha = 1.9444$  line with the upper and lower thick solid lines in Figure 3.2, respectively. For  $\alpha$ 's within  $\sim 1\%$  of 1.9444 equations 7-8 are a good approximation to the actual solutions of the Jeans equation. For other values, the approximation is less valid. For example, for  $\alpha = 1.875$  the above expression is shown as the thin long-short-dash line in Figure 3.4. For reference, we plot the value of  $\gamma_0$ , the slope where the density slope changes most rapidly, as a thin solid line in Figure 3.2. As expected, for  $\alpha = 1.9444$ ,  $\gamma_0 = \gamma_{pl} = 2.111$ .

Finally, we note that  $\alpha = 1.9444$  periodic solution value applies to the case of isotropic velocity dispersion,  $\beta = 0$ . If a halo is characterized by a larger, but constant anisotropy, the periodic  $\alpha$  value decreases. In the limiting case of radial orbits and  $\beta = 1$ ,  $\alpha = 1.7222$ . Dark matter halos with non-zero anisotropy will be discussed in a future paper.

### 3.5. Two classes of solutions

It is clear from Figure 3.4 that  $\alpha = 1.9444$  is the watershed value that separates two different types of Jeans equation solutions: an example of  $\alpha > 1.9444$  is the short-dash line spiral curve that eventually settles to a constant finite value of  $\gamma$ ; an example of  $\alpha < 1.9444$  is the solid line which shows a rapid increase of  $\gamma$  to very large values. The damping term line,  $8\alpha - 5\gamma - 5 = 0$  in Figure 3.2 explains this behavior. Solutions with  $\alpha < 1.9444$  tend to have a negative average damping term (and density profiles that steepen without limit), while solutions with  $\alpha > 1.9444$  tend to experience positive average damping (and result in density profiles that asymptote to power-laws, albeit at very large radii). We will call these the negative and positive damping solutions, respectively.

Let us consider negative damping solutions and, for concreteness, set  $\alpha = 1.875$ . We integrate equation 5 from the center of a halo outward, i.e. from small to large values of  $\ln x$ . We start from  $\gamma_{in}$  given by  $2\alpha - 5\gamma = 0$ , and  $\gamma'$  slightly greater than 0, which ensures that the center of the halo will have constant density profile slope,  $\gamma_{in} = (2/5)\alpha$ , and hence vanishing pressure gradient (Section 3.2). As  $\ln x$  increases,  $\gamma$  increases without limit, because of the negative average damping term. The solid thick line in Figure 3.4 shows the resulting profile. The same profile is also shown in Figure 3.4 with the same line type. (Note that the horizontal normalization is not important, and was adjusted for easier comparison between various results.)

To illustrate the behavior of positive damping term solutions we set  $\alpha = 1.975$ . As before, we choose  $\gamma_{in} = (2/5)\alpha$ , and initial  $\gamma'$  slightly greater than 0. This solution is

plotted as the short-dash line in Figures 3.4 and 3.4. It does not attain steep density slopes in the outer halo;  $\gamma$  climbs to about 2.45, then oscillates, with decreasing amplitude, and eventually settles to the asymptotic value given by  $2\alpha + \gamma_{pl} - 6 = 0$ . It is the positive average damping term in equation 5 that forces the oscillations to a constant asymptotic  $\gamma_{pl}$ .

Thus, the behavior of  $\gamma$  vs.  $\ln x$  for  $\alpha$  greater and less than the periodic value (1.9444) are qualitatively different. If  $\alpha < 1.9444$  the outer density slope increases without limit, while if  $\alpha > 1.9444$  there is a maximum value for  $\gamma$ , followed by oscillations.

If we abandon the  $\gamma'_{in} \gtrsim 0$  initial condition and instead use  $\gamma'_{in} > 0$  we can “overpower” the positive damping term and make  $\gamma$  attain large values. The solution obtained with  $\gamma'_{in} = 1.05$  and  $\alpha = 1.975$  is plotted as the long-dash line in Figure 3.4. The price we pay for resorting to large  $\gamma'_{in}$  is non-zero  $d \ln(\rho\sigma^2)/d \ln r$  at the center of the halo. (Furthermore,  $\gamma$  decreases towards the center, and becomes negative: these halos have density holes in the center.) It is impossible to make a halo with  $\alpha > 1.9444$ , constant pressure core, and outer halo  $\gamma > 3 - 4$  within the confines of the spherically symmetric, isotropic velocity dispersion Jeans equation.

### 3.5.1. NFW vs. Hernquist-type density profiles

We illustrate the positive and negative damping solutions with Hernquist and NFW density profiles, respectively. The recent work of Kazantzidis et al. (2004) provides us with N-body realizations of Hernquist (their Model D) and NFW (Model F) profiles. These halos are not the result of the usual cosmological evolution starting from small density perturbations; instead they were explicitly constructed as isolated equilibrium objects. To qualify for the analysis using equation 5 the halos must be in equilibrium, have isotropic velocity dispersion ellipsoids, and power-law phase-space density distributions. Models D and F meet all three requirements. The N-body generated halos have been evolved for 50 crossing times and thus have been explicitly shown to be in equilibrium. The velocity ellipsoid parameter,  $\beta$ , equation 1, is zero for Models D and F. To estimate the phase-space density distribution we used Figure 3 of Kazantzidis et al. (2004) to measure density and velocity dispersion profiles at seven points over 2-2.5 decades in radius.

The phase-space density distribution of Model D is reasonably approximated by a power-law: the slope based on the inner half of the halo is  $\alpha = 2.01$ , while the outer half has  $\alpha = 2.53$ . The average over the whole halo is with  $\alpha = 2.27 \pm 0.11$ ; the error is the RMS dispersion about the best fit line. We use this  $\alpha$  value to generate the Jeans equation solution, and plot it as the dot-dash line in Figure 3.4. The solution and the actual data points from Kazantzidis et al. (2004) (empty squares) are in very good agreement. For reference, we also plot the Hernquist density profile,  $\rho \propto [x(1+x)^3]^{-1}$ , as a thin solid line.

The phase-space density profile of Model F is well fit by a single power-law with  $\alpha = 1.95 \pm 0.04$ . This value is in excellent agreement with the periodic solution  $\alpha = 1.9444$  that we derived from the Jeans equation in Section 3.4. Since Kazantzidis et al. (2004) did not set out to produce halos with  $\alpha$  close to the periodic value, we speculate that 1.9444 is an attractor, albeit a weak one: halos whose properties are already close to those of the periodic solution (because of input constraints, dynamical evolution, or some other reason), end up with  $\alpha \approx 1.9444$ . The range of  $\alpha$  values exhibited by the ESIM halos in Section 2 also attests to the weakness of the “periodic solution” attractor.

The density profile of Model F (solid dots in Figure 3.4) can be reproduced with the Jeans equation solution with  $\alpha = 1.95$  and large  $\gamma'_{in}$ , around 1, or with a smaller  $\alpha$  and  $\gamma'_{in} = 0$ . For example,  $\alpha = 1.875$  and  $\gamma'_{in} = 0$  solution is plotted as a thick solid line; the NFW empirical fit (thin solid line) is plotted for reference.

While the Model F value of  $\alpha = 1.95 \pm 0.04$  is fully consistent with the periodic solution, it is inconsistent with TN01’s 1.875 at  $\sim 2\sigma$ . There are at least two possibilities why the  $\alpha$  value obtained from N-body simulations deviates from the periodic solution obtained assuming symmetric, isotropic halos in perfect hydrostatic equilibrium. N-body halos are subject to dynamical evolution, like gravitational collapse and mergers. Any of these could drive  $\alpha$  away from the periodic solution value. Alternatively, it is possible that our assumption of zero velocity dispersion anisotropy is not a good enough approximation. The actual anisotropy in halos has a gradient, with the inner region being isotropic and outer regions being more radial (Barnes et al. 2005a). Extending equation 5 from  $\beta = 0$  to  $\beta \neq 0$ , one can show that constant positive anisotropy will shift the periodic solution to smaller  $\alpha$  values;  $\alpha = 1.875$  is the periodic solution for  $\beta = 0.3125$  equilibrium halo. We postpone a detailed treatment of velocity anisotropy to a later paper. Finally, there are other, more subtle issues that can drive  $\alpha$  away from its periodic value; halo triaxiality is one example.

### 3.6. Conclusions from the Jeans equation analysis

Our goals in Section 3 were two-fold: gain insight into the properties of solutions of the Jeans equation, and find out if the Jeans equation singles out any value of  $\alpha$ . Analyzing equation 5 we found that the isotropic Jeans equation does indeed point to a special  $\alpha$ :  $\alpha = 1.9444$  results in periodic variation of  $\gamma$  vs.  $\ln x$ . Thus,  $\alpha = 1.9444$  divides the solutions into those where the damping term is typically negative, and  $\gamma$  increases without limit, producing halos with density profiles that steepen at large radii, and those where the damping term is typically positive, and  $\gamma$  asymptotes to a constant value, and hence power-law density profiles (provided the initial  $\gamma'$  is small).

For halos with constant non-zero velocity anisotropy,  $\beta$ , the periodic solution shifts to smaller values of  $\alpha$ ; halos with purely radial orbits have periodic  $\alpha = 1.7222$ . The N-body

simulated halos have average anisotropies between 0 and 1; so the corresponding periodic solution  $\alpha$  is bracketed by 1.7222 and 1.9444. Given this information, it is not surprising that the N-body generated halos that have  $\beta > 0$  and have undergone considerable dynamical evolution are characterized by an intermediate  $\alpha \approx 1.88$  (see Section 3.5.1). Our own tests with ESIM halos (Section 2) produce a range of  $\alpha$  values, depending on the parameters of the initial set-up, and the properties of final halos. In a sense, ESIM halo results agree with the conclusions from the Jeans equation analysis because neither predict that all halos should have the same  $\alpha$ . Based on the analysis of Section 2 and 3 we conclude that the radial slope of the phase-space density,  $\alpha$ , is not fixed by the condition of hydrostatic equilibrium, and so must be the result of some other physics.

#### 4. Conclusions

Examination of a handful of N-body dark matter halos indicates that the phase-space density,  $\rho/\sigma^3$ , is a power-law in radius, even though the density profile is not (Taylor & Navarro 2001). To determine if the scale-free nature of  $\rho/\sigma^3$  is peculiar to N-body halos (may be even just those presented in TN01), or is a more generic outcome of collisionless gravitational collapse, we turned to a different method of generating equilibrium halos. The Extended Secondary Infall Model (ESIM) halo formation, which we used in Section 2, proceeds very differently from that of N-body simulations. ESIM halos are spherically symmetric, and non-rotating. By assumption, the collapse conserves the angular and radial momenta of all shells individually. The final equilibrium halos are supported against collapse by radial and tangential velocity dispersion.

Despite the differences between N-body and ESIM methods, and the resulting density profiles, both types of halos are characterized by a scale-free  $\rho/\sigma^3$  profile. We speculate that because this feature is common to the two types of halos, it is an outcome of the one piece of physics shared by the two methods: violent relaxation. At the very least violent relaxation is a sufficient, if not the necessary condition needed to produce  $\rho/\sigma^3 \propto r^{-\alpha}$ . We will further test this hypothesis in subsequent work.

If the scale-free nature of  $\rho/\sigma^3$  is, in fact, a generic feature of collisionless halos, it implies an additional constraint on the halo structure as the density and velocity dispersion profiles are now closely related. In particular, the analysis of the Jeans equation and subsequent implications for halo formation are now not as unconstrained as before. Using this additional condition, we have rewritten the second derivative of the Jeans equation as equation 5, and used it as the starting point of our analysis in Section 3. This analysis yielded some interesting and novel insights into the solutions of the Jeans equation. In particular, we identified the unique periodic solution of equation 5, where the halo density profile slope oscillates between some minimum and maximum value. The corresponding  $\alpha = 1.9444$  is

the only special  $\alpha$  value admitted by the spherically-symmetric, isotropic Jeans equation.

In the future, we plan to extend the analysis of the Jeans equation to include non-zero velocity dispersion anisotropy distributions. Our ultimate goal is to identify the physical processes that shape the dark matter halos produced in simulations, and eventually, in the real Universe.

This work was supported in part by NSF grant AST 03-07604. AB also receives research support from the Natural Sciences and Engineering Research Council (Canada) through the Discovery grant program. He further acknowledges support from the Leverhulme Trust (UK) in the form of the Leverhulme Visiting Professorship at the Universities of Oxford and Durham, where part of this work was carried out. JJD was partially supported through the Alfred P. Sloan Foundation. The authors are grateful to Adi Nusser for his insightful comments.

### A. Convex density profile solutions of the Jeans equation

All density profiles that appear in the literature and describe mass (or light) distribution in galaxies are “concave”, i.e. the double logarithmic density slope steepens with radius,  $\gamma' > 0$ . However, the Jeans equation also admits solutions with  $\gamma' < 0$ . These can be obtained by integrating equation 5 starting with  $\gamma_{in}$  given by  $\frac{2}{3}[\alpha - \gamma] + 1 = 0$  and  $\gamma'_{in} \lesssim 0$ . The density profiles asymptote to constant  $\gamma_{in} = \alpha + 1.5$  at the center, and constant  $\gamma_{out} = (2/5)\alpha$  in the outer parts. In the representation of Figure 3.2 these profiles start at the upper thick solid line and end at the lower thick solid line. For any value of  $\alpha$  the exact analytical solution is,

$$\gamma' = -\gamma'_m + \frac{2}{3}(\gamma - \gamma_0)^2, \quad \gamma_0 = (14\alpha + 15)/20, \quad \gamma'_m = 3(2\alpha + 5)^2/200, \quad (A1)$$

and the double logarithmic density profile slope is given by

$$\gamma = -(3\gamma'_m/2)^{1/2} \tanh [(2\gamma'_m/3)^{1/2} \ln x] + \gamma_0. \quad (A2)$$

The form of these equations is similar to that of equations 7-8 that describe concave density profiles (Section 3.4). The value of the density profile slope where the density slope changes most rapidly,  $\gamma_0$ , is depicted by a thin solid line in Figure 3.2. An example of this type of density profile is the lower half ( $\gamma' < 0$ ) of the long dash line in Figure 3.4. In these halos the velocity dispersion,  $\sigma$ , after reaching its minimum value at the radius where  $\gamma = \gamma_0$ , starts to increase in the outer parts of the halo. The pressure,  $\rho\sigma^2$ , asymptotes to a constant in the outer parts because  $\gamma_{out} = (2/5)\alpha$  is constant there (see Section 3.2).

## B. Phase-space density of halos and the secondary infall model

In Section 2 we examined the phase-space density of halos formed via the Extended Secondary Infall Model, ESIM, which differs from the original, Secondary Infall Model, SIM (Gunn & Gott 1972; Gott 1975) in many respects. The most notable differences are the shape of the pre-collapse peak (extended in ESIM, point mass in SIM), and the inclusion of secondary perturbations, and hence random motions in the ESIM (SIM halo collapse is purely radial). With these differences in mind, it is interesting to compare  $\alpha$  values obtained in Section 2 to the prediction of SIM.

In a spherically symmetric SIM halo collapse proceeds as follows. Initially, a small constant central mass excess,  $\delta M_0$  is surrounded by material of average density. The dynamics of the pre-turn-around period is described by the parametric equations,  $r \propto (1 - \cos \theta)$ , and  $t \propto (\theta - \sin \theta)$ . The maximum radius for a shell of initial comoving radius  $r_i$  is  $r_m = r_i \bar{\delta}^{-1}$ , where  $\bar{\delta}$  is the initial fractional overdensity inside  $r_i$ . Enclosed mass,  $M(< r_i) \propto \rho r_i^3$ , so  $r_i \propto M^{1/3}$ . And,  $\bar{\delta} = \delta M_0 / M \propto M^{-1}$ . Combining these scalings we get  $r_m \propto M^{4/3}$ , for each shell in the halo. After reaching turn-around, a shell collapses back somewhat; it is usually assumed that the collapse factor, i.e. the ratio of the turn-around radius,  $r_m$ , to the final radius in the virialized halo, is the same for all shells. Further assuming that each shell spends most of the time at its apocenter, which is proportional to  $r_m$ , one derives the resulting density distribution in the final virialized halo:  $\rho(r) \propto r^{-2} dM/dr$ , or,  $\rho \propto M^{-3} \propto r_m^{-9/4}$ . This is a well known result.

Let us take this approach a little further. In the real Universe the collapse of material will not be purely radial; there will be some random motion of particles, and associated kinetic energy. If we assume that during the collapse the kinetic energy is derived from the gravitational potential energy of infalling material, then the two types of shell energy are proportional, and  $\frac{1}{2}v^2 \propto GM/r_m$ . Kinetic energy of random motion gives an estimate of the velocity dispersion:  $\sigma \propto (M/r_m)^{1/2} \propto r_m^{-1/8}$ . Combining  $\rho(r)$  from the previous paragraph with  $\sigma(r)$ , we get the radial dependence of the phase-space density,  $\rho/\sigma^3 \propto (r^{-9/4})/(r^{-3/8}) \propto r^{-15/8}$ , i.e.  $\alpha = 1.875$ . If the kinetic energy is not simply proportional to the potential energy, the final value of  $\alpha$  will differ accordingly. The SIM phase-space density shape is always a power-law, by definition.

These are the predictions of the highly simplified SIM. Given that ESIM halos of Section 2 have more complexity, and a variety of initial conditions, it is not surprising that ESIM halos show a wide range of  $\alpha$  values. However, the typical values are not far from the SIM prediction of 1.875. Finally, the fact that  $\alpha = 1.875$  derived here, has the same numerical value as the best-fit  $\alpha$  quoted by Taylor & Navarro (2001) for their N-body generated halos, is probably a coincidence, because the hierarchical halo formation characteristic of N-body simulations is qualitatively different from the highly idealized SIM.

## REFERENCES

Avila-Reese, V., Firmani, C. & Hernndez, X. 1998, *ApJ*, 505, 37

Bardeen, J.M., Bond, J.R., Kaiser, N. & Szalay, A.S. 1986, *ApJ*, 304, 15

Barnes, E.I., Williams, L.L.R., Babul, A. & Dalcanton, J.J. 2005a, in preparation

Barnes, E.I., Williams, L.L.R., et al. 2005b, in preparation

Bertschinger, E. 1985, *ApJS*, 58, 39

Binney, J. & Tremaine, S. 1987, *Galactic Dynamics* (Princeton: Princeton University Press)

Dehnen, W. 2005, preprint, astro-ph/0504246

Diemand, J., Zemp, M., Moore, B., Stadel, J. & Carollo, M. preprint, astro-ph/0504215

Gott, J.R. 1975, *ApJ*, 201, 296

Gunn, J.E. & Gott, J.R. 1972, *ApJ*, 176, 1

Hansen, S. H. 2004, *MNRAS*, 352, L41

Huss, A., Jain, B. Steinmetz, M. 1999, *ApJ*, 517, 64

Kazantzidis, S., Magorrian, J., Moore, B. 2004, *ApJ*, 601, 37

Merritt, D., Navarro, J.F., Ludlow, A. & Jenkins, A. preprint, astro-ph/0502515

Moore, B., Governato F., Quinn, T., Stadel, J. & Lake, G. 1998, *ApJ*, 499, L5

Moore, B., Quinn, T., Governato F., Stadel, J. & Lake, G. 1999, *MNRAS*, 310, 1147

Navarro, J.F., Frenk, C.S. & White, S.D.M. 1997, *ApJ*, 490, 493

Navarro, J.F. et al. 2004, *MNRAS*, 349, 1039

Ryden, B. S., Gunn, J. E. 1987, *ApJ*, 318, 15

Syer, D. & White S. D. M. 1998, *MNRAS*, 293, 337

Taylor, J.E. & Navarro, J.F. 2001, *ApJ*, 563, 483

Williams, L.L.R., Babul, A. & Dalcanton, J.J. 2004, *ApJ*, 604, 18

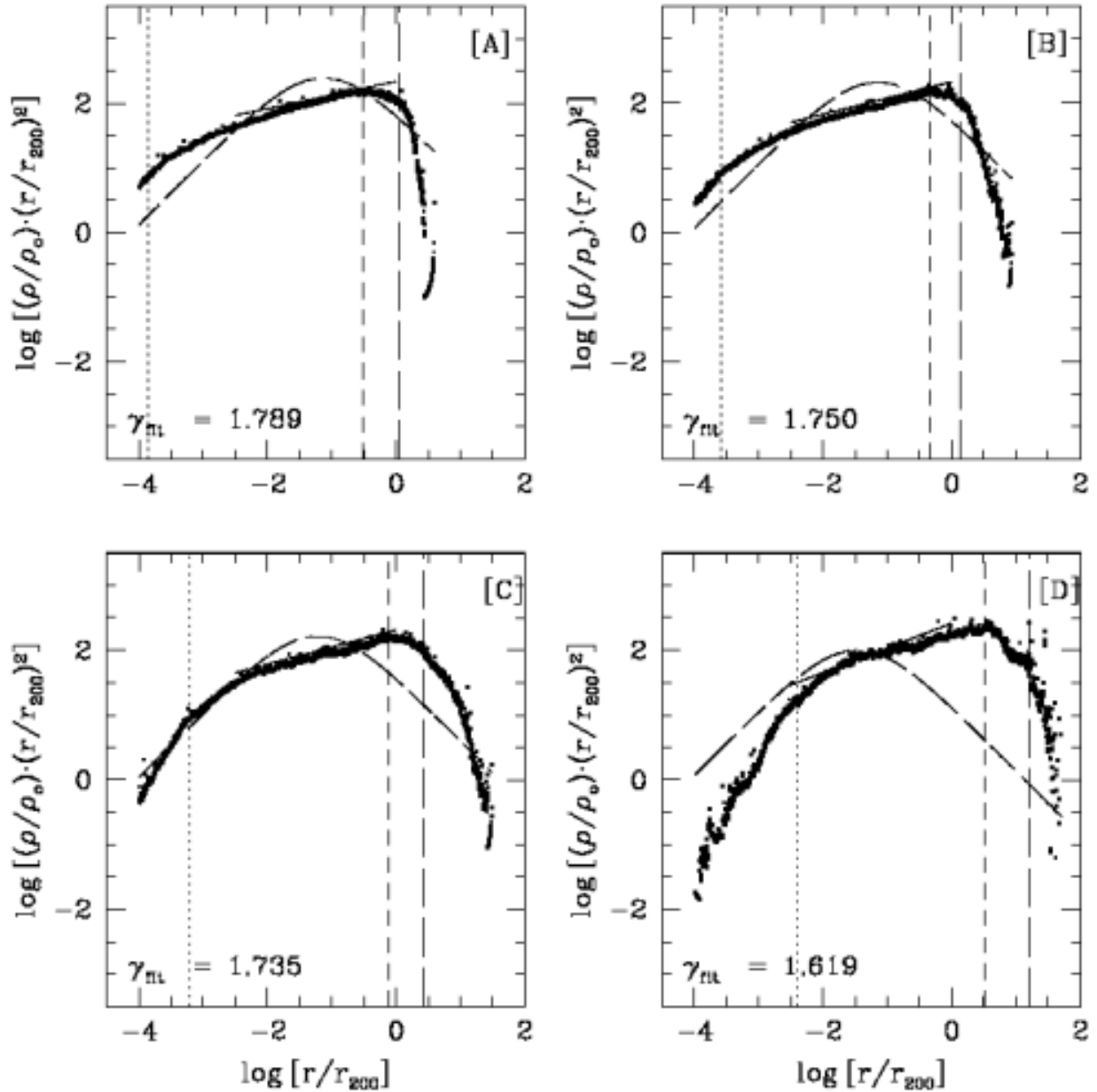


Fig. 1.— Density vs. radius in units of the virial radius,  $r_{200}$ , for galaxy-mass halos generated with  $r_h = 0.05\text{Mpc}$ , and perturbation amplitude scaling parameters of 0.4 [A], 0.6 [B], 1 [C], and 2 [D]. The density has been normalized by the critical density at the present epoch, and multiplied by  $(r/r_{200})^2$ . The NFW profile is over-plotted as a long dash line in all 4 panels. The NFW concentration parameters were computed using the masses of the corresponding halos. The dotted, short dash and long dash lines represent radii where the density slope is 1, 2 and 3;  $r_{\gamma=1,2,3}$ . Each profile is fitted with a power-law between  $10^{-2.5}$  and 1 virial radius (thin solid lines); the value of the best-fit slope is noted in each panel.

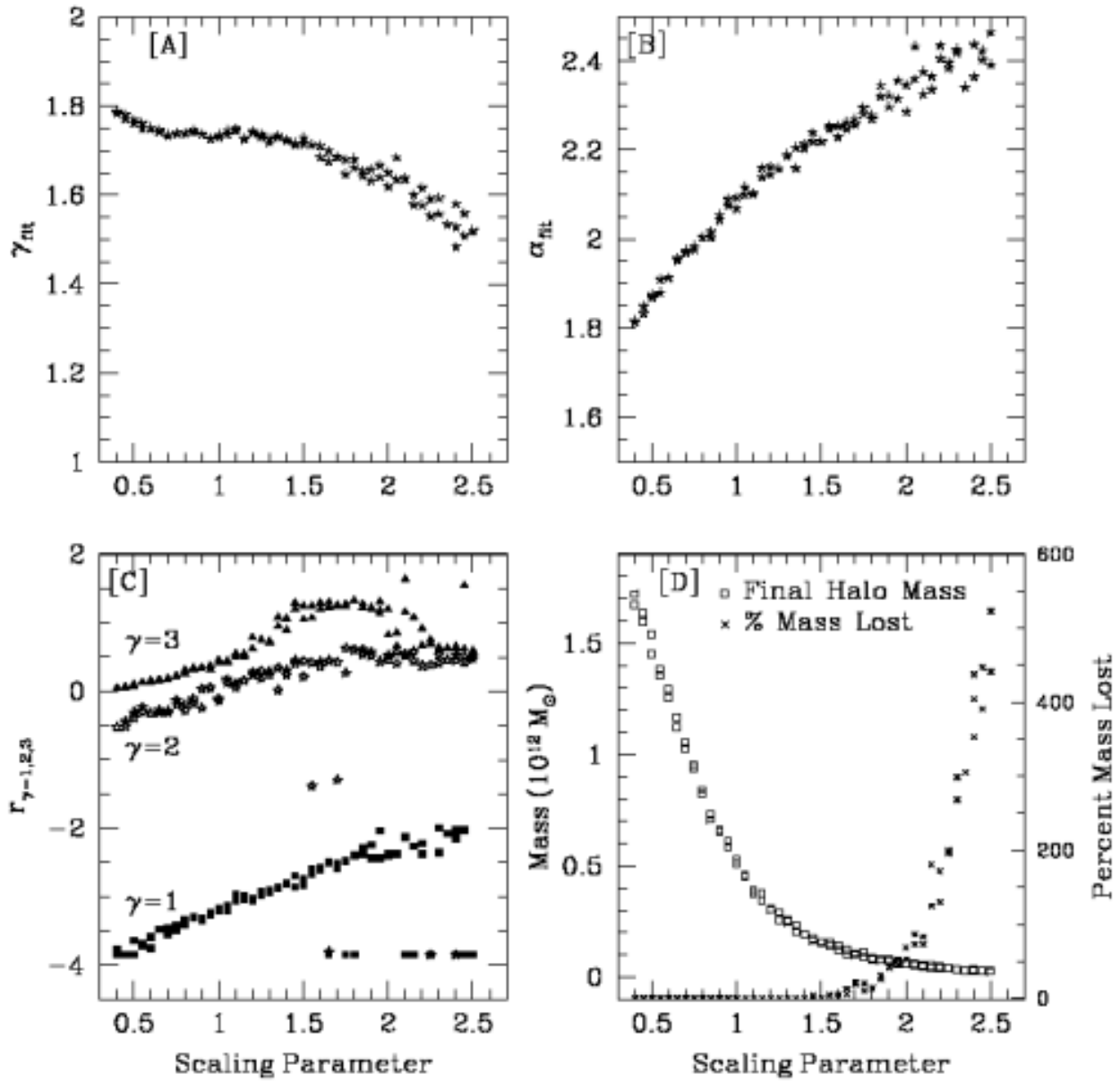


Fig. 2.— The final properties of galaxy-mass halos with  $r_h = 0.05\text{Mpc}$  as a function of the perturbation amplitude scaling parameter. [A]: Slope of the log-log density profile,  $\gamma_{fit}$ ; [B]: Slope of the log-log  $\rho/\sigma^3$  profile,  $\alpha_{fit}$ ; [C]:  $r_{\gamma=1}$ ,  $r_{\gamma=2}$ , and  $r_{\gamma=3}$ : radii, in terms of virial, where the double logarithmic density slopes attain values of 1, 2, and 3, respectively; [D]: Virial mass of the halo (squares, and left vertical axis) and percentage mass lost during formation, with respect to the final halo mass (crosses, and right vertical axis). Note that as the amplitude of secondary perturbations is increased, the resulting halos have shallower density slopes ([A] and [C]) due to increased angular momentum, steeper phase-space density slopes [B], and more mass loss [D] due to the increased probability of matter reaching escape velocity.

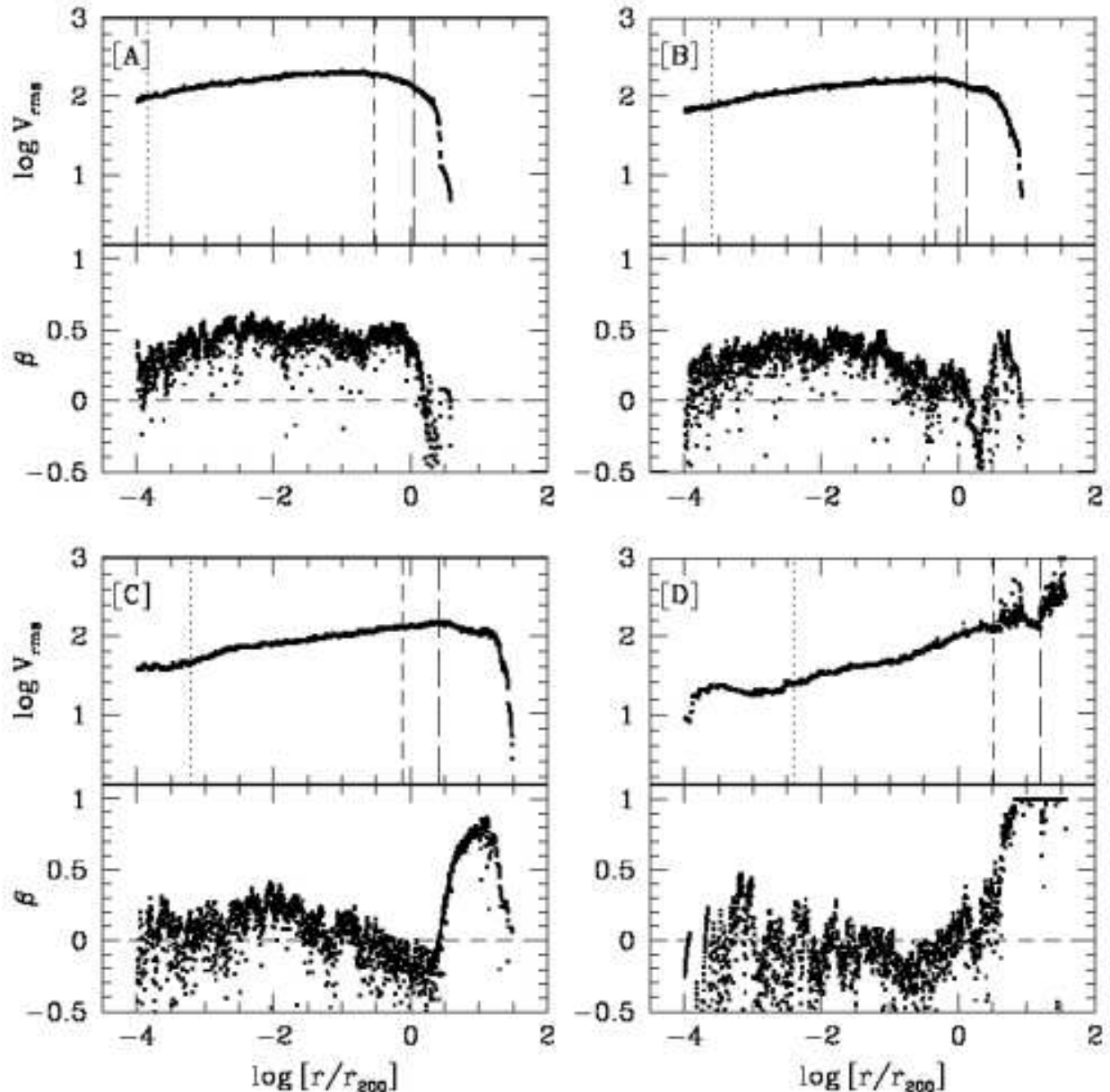


Fig. 3.— The top half of each of the four panels shows the RMS velocity profile for halos with perturbation amplitude scaling parameters of 0.4 [A], 0.6 [B], 1 [C], and 2 [D]. The lower half of each panel shows the velocity dispersion anisotropy,  $\beta$ . Again, the values of  $r_{\gamma=1,2,3}$  are shown in dotted, short dash, and long dash lines. Halos [A] and [B] have somewhat radial velocity anisotropies, while halos [C] and [D] have nearly isotropic velocity dispersions.

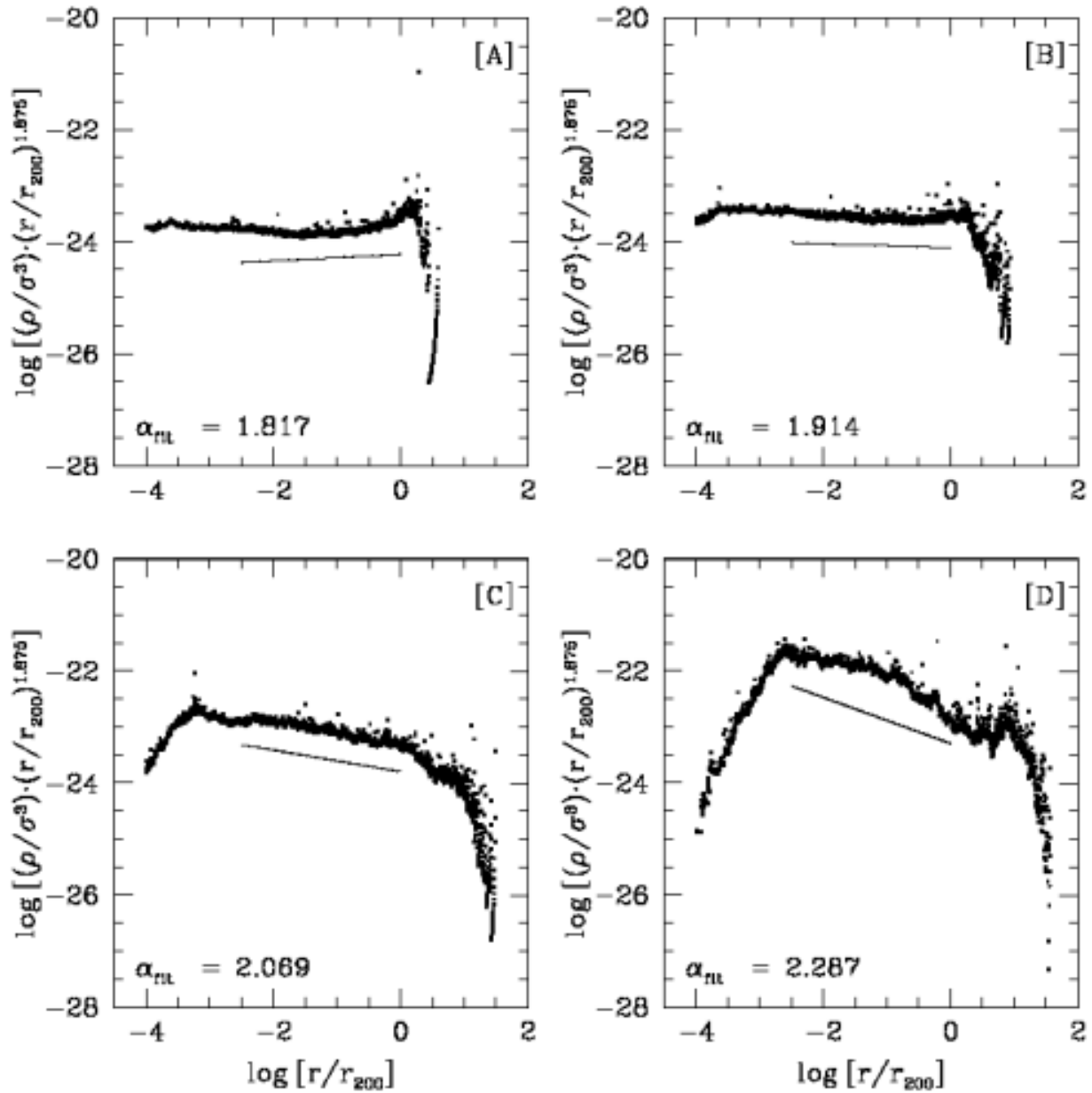


Fig. 4.— The phase-space density profiles of halos with perturbation amplitude scaling parameters of 0.4 [A], 0.6 [B], 1 [C], and 2 [D]. The  $\rho/\sigma^3$  data have been multiplied by  $(r/r_{200})^{1.875}$ . TN01's fit would be represented here by a horizontal line. The short thin lines above the data indicate our linear least-squares fit between  $10^{-2.5}$  and 1 virial radius. The value of the power-law index fit is indicated in each panel. Note the nearly scale-free behavior for 2-3 decades in radius.

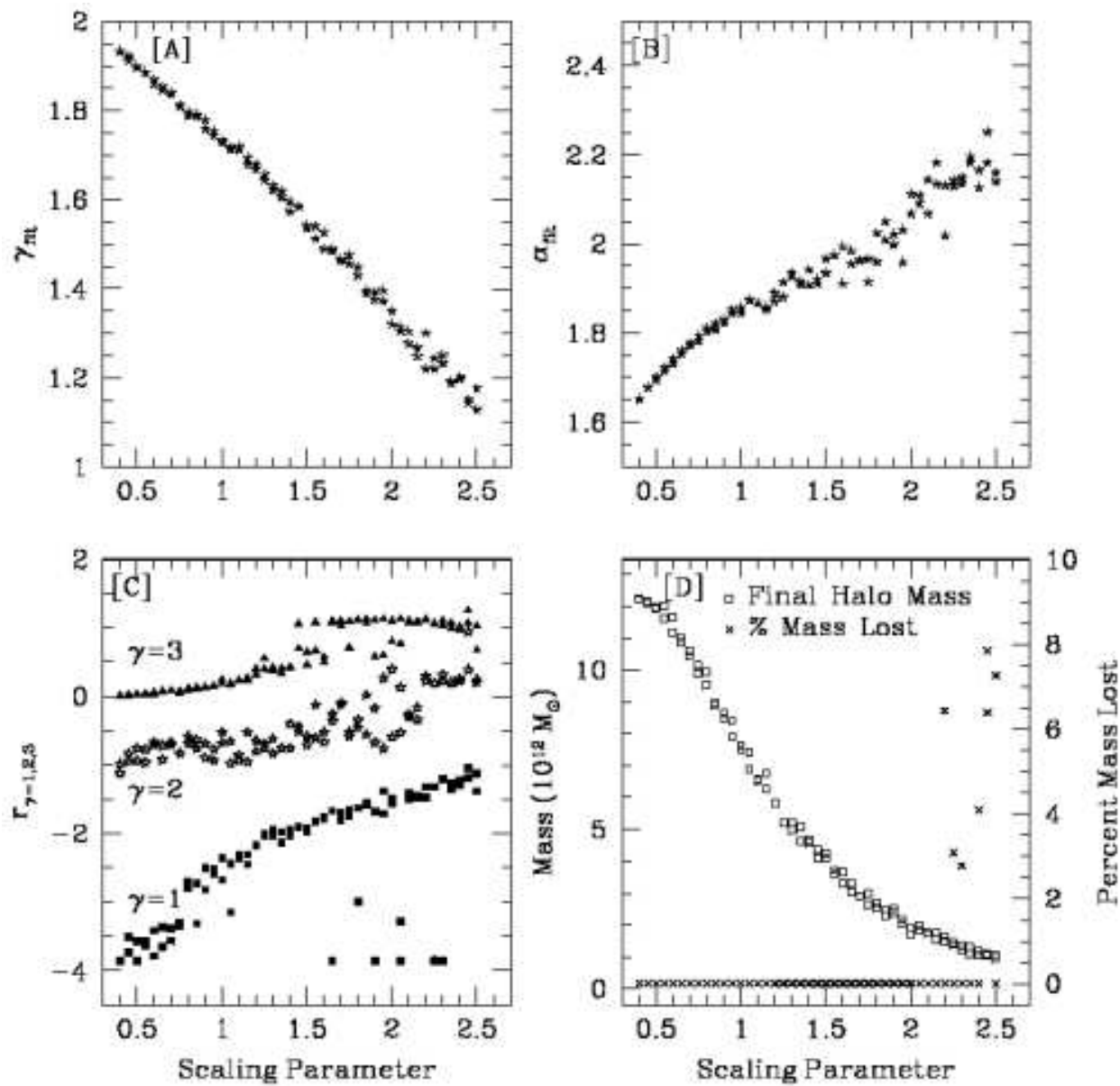


Fig. 5.— Same as Figure 2.2.1, but for group-mass halos with  $r_h = 0.35\text{Mpc}$ .

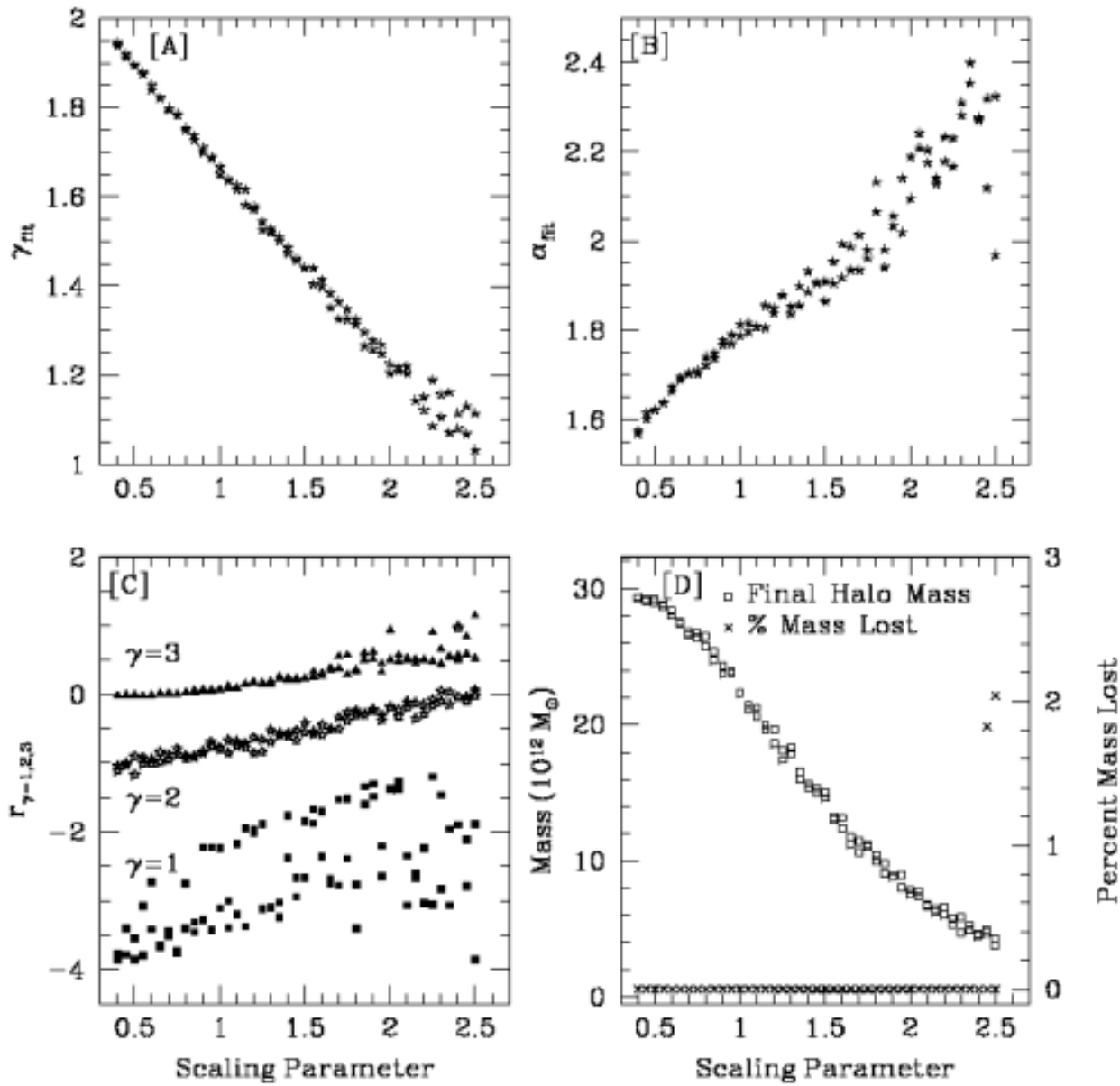


Fig. 6.— Same as Figure 2.2.1, but for cluster-mass halos with  $r_h = 0.7 \text{ Mpc}$ .

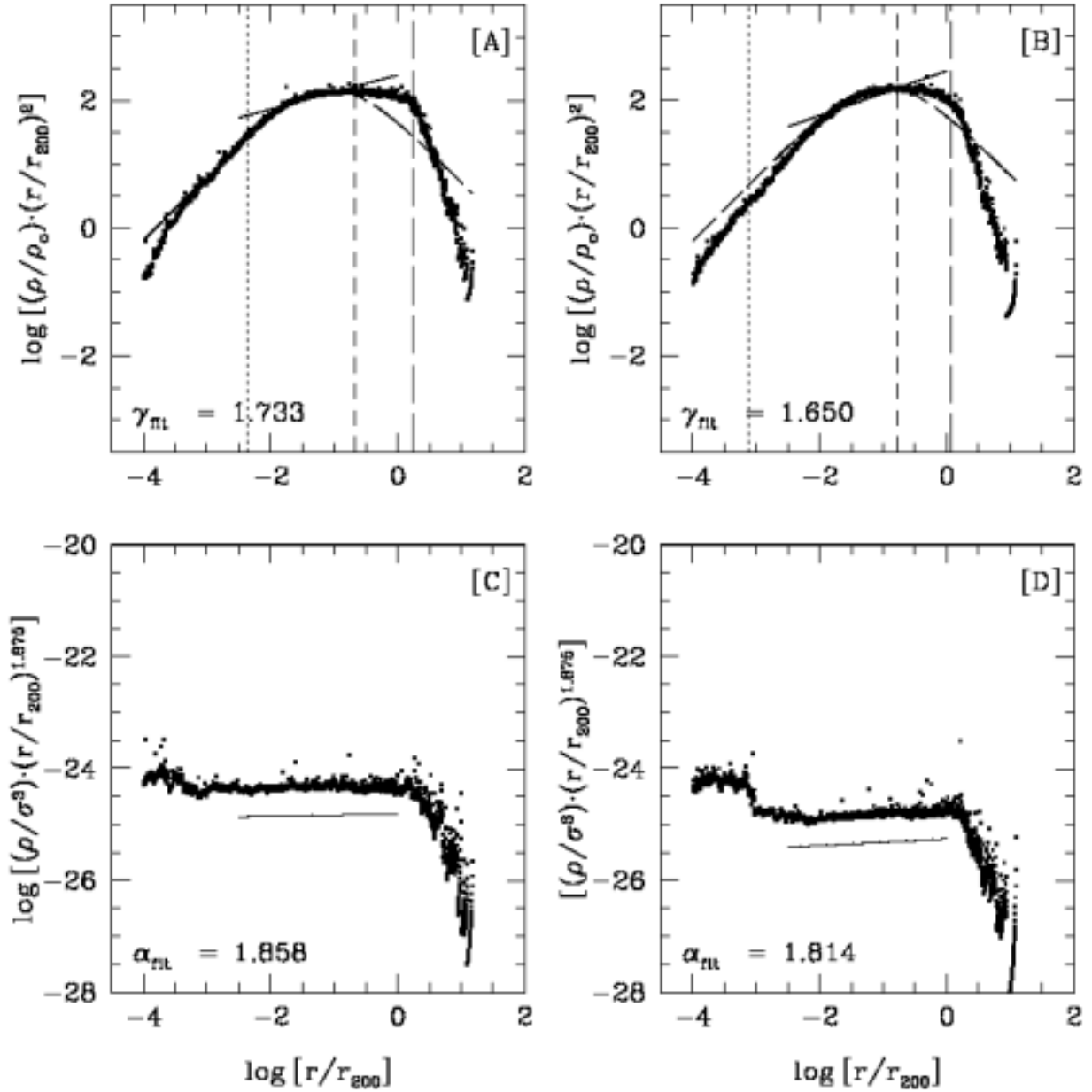


Fig. 7.— The density (top panels) and phase-space density (bottom panels) profiles of two halos, both having scaling parameter of 1, generated with  $r_h = 0.35\text{Mpc}$  (panels [A] and [C]) and  $r_h = 0.7\text{Mpc}$  (panels [B] and [D]). For comparison, we show the NFW formula in the two top panels (long dash line), with the concentration parameter appropriate for that halo. Note that the phase-space density profiles are well fit by power-laws, while the density profiles are not.

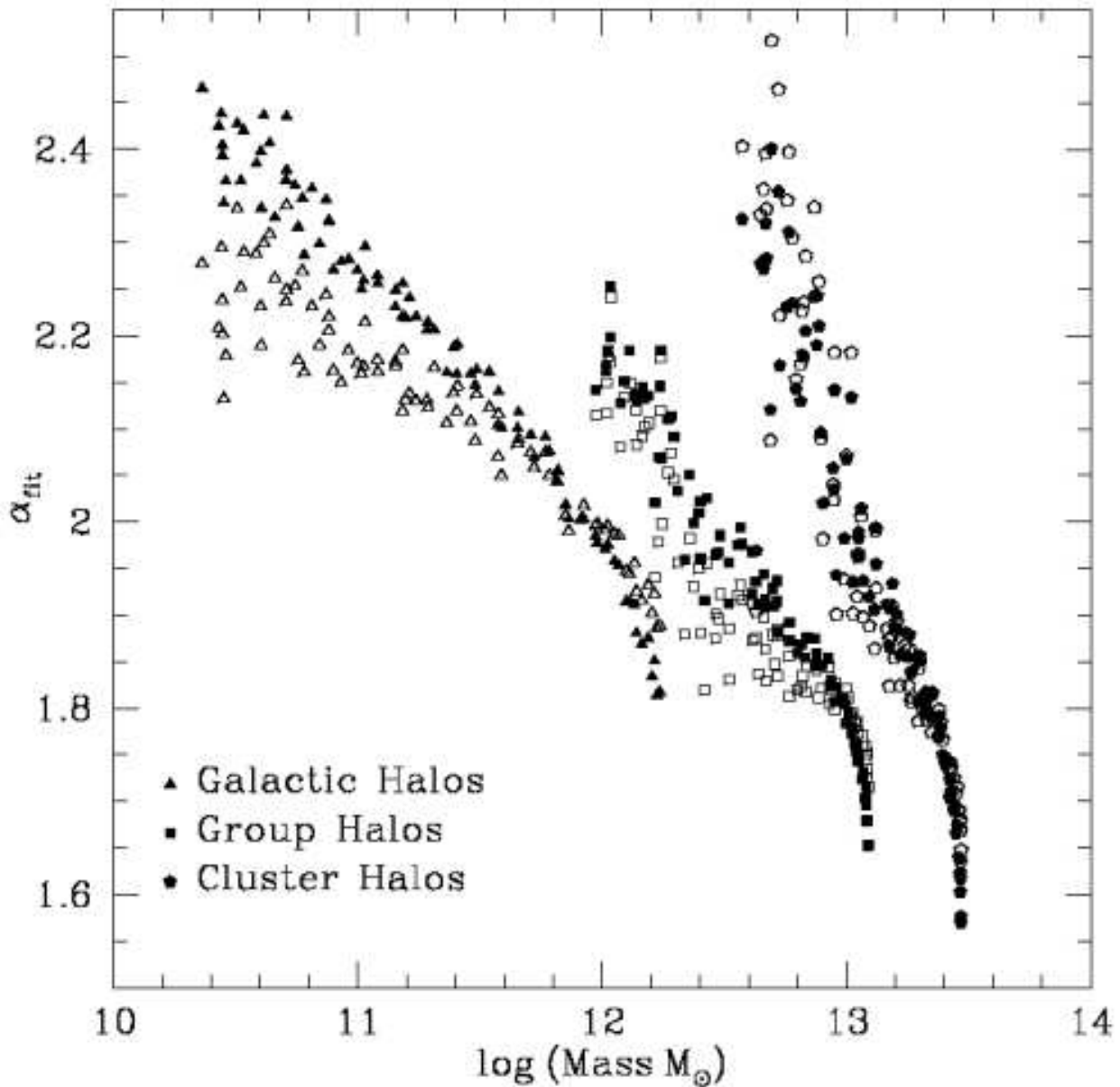


Fig. 8.— The double logarithmic slope,  $\alpha_{fit}$ , of  $\rho/\sigma^3$  vs. radius, as a function of the virial halo mass, for three different  $P(k)$  filtering scales,  $r_h = 0.05, 0.35$  and  $0.7\text{Mpc}$  (triangles, squares, and pentagons). Filled (empty) symbols show  $\alpha_{fit}$  values computed using  $10^{-2.5} \rightarrow 1$  ( $10^{-2.5} \rightarrow 10^{-0.5}$ ) radial range, given in terms of  $r_{200}$ . Note that  $\alpha_{fit}$  is not uniquely determined by halo mass, amplitude of secondary perturbations, halo filtering scale, etc.

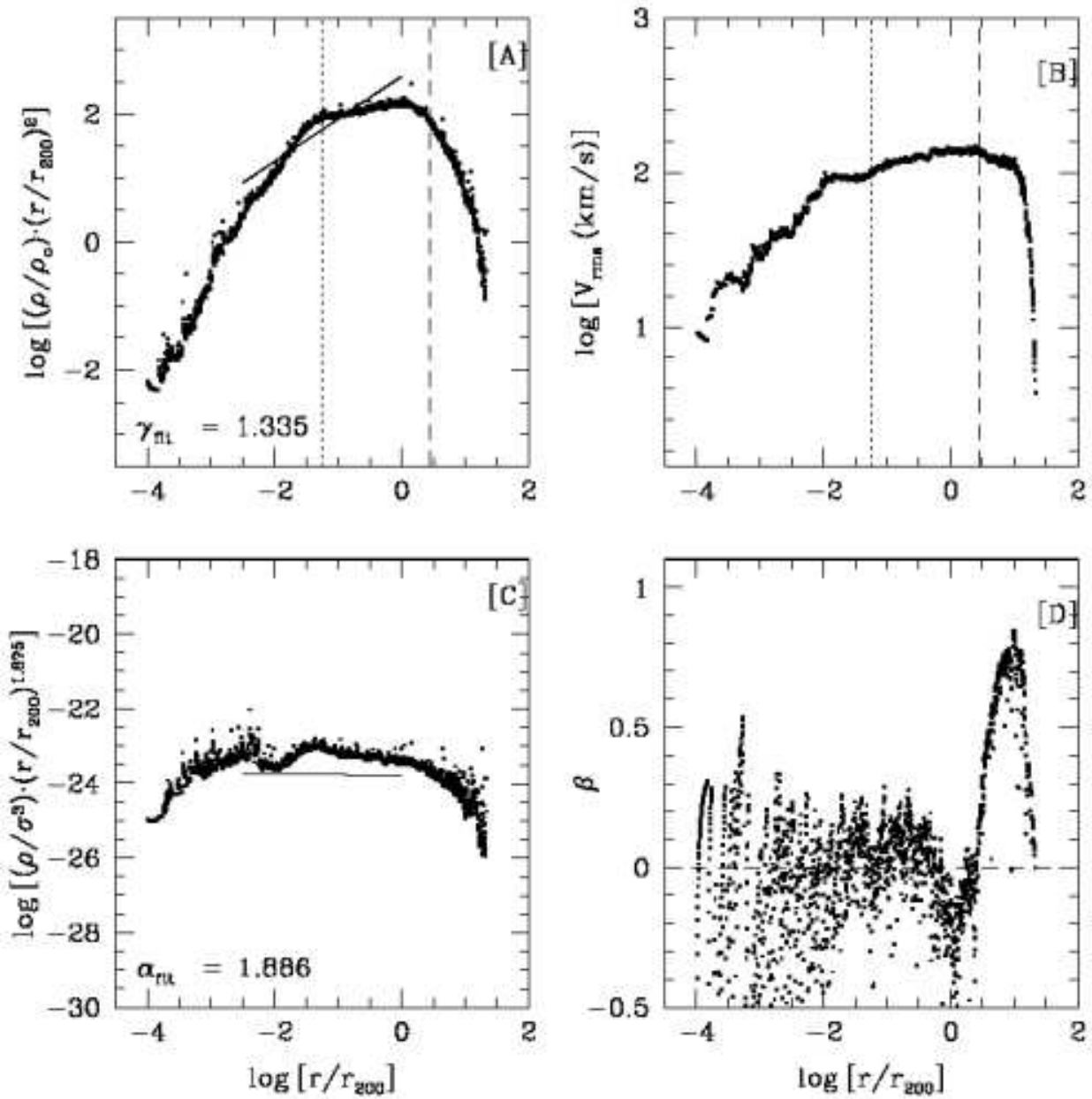


Fig. 9.— An example of a halo with discontinuous perturbation amplitude scaling parameters: shells with the initial comoving radii between 0.59 and 0.79 Mpc were assigned a scaling parameter of 5, while the rest of the halo, all the way up to the last shell at 1.92 Mpc were assigned a scaling parameter of 0.9. [A]: Density profile, multiplied by  $(r/r_{200})^2$ ; [B]: RMS velocity dispersion profile; [C]: Phase-space density profile, multiplied by  $(r/r_{200})^{1.875}$ ; [D]: Velocity dispersion anisotropy profile,  $\beta$ . This halo illustrates that the scale-free nature of  $\rho/\sigma^3$  is a resilient feature of virialized halos: even in halos with discontinuous scaling parameters, density [A] and velocity dispersion [B] track each other, with the result that  $\rho/\sigma^3$  is reasonably well fit by a power-law [C].

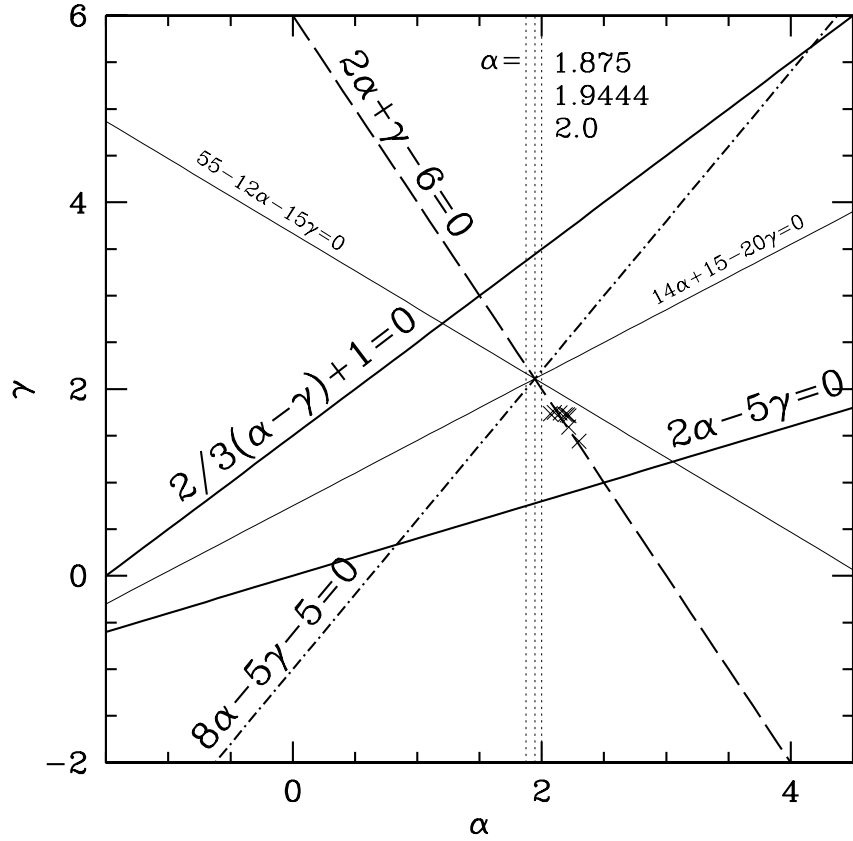


Fig. 10.— Pictorial depiction of equation 5. Thick solid and long-dash lines represent the terms on the LHS of equation 5. The dot-dash line is the coefficient of the damping term on the RHS of equation 5. The two thin solid lines are  $\gamma_0(\alpha)$ 's given in equations 7 and A1. The three vertical dotted lines at  $\alpha = 1.875, 1.9444$  and 2 are plotted to guide the eye. Periodic solutions are obtained for  $\alpha = 1.9444$  (Section 3.4). A set of closely spaced crosses are  $\alpha_{fit}$  and  $\gamma_{fit}$  values for galaxy-mass ESIM halos with  $\beta \approx 0$ .

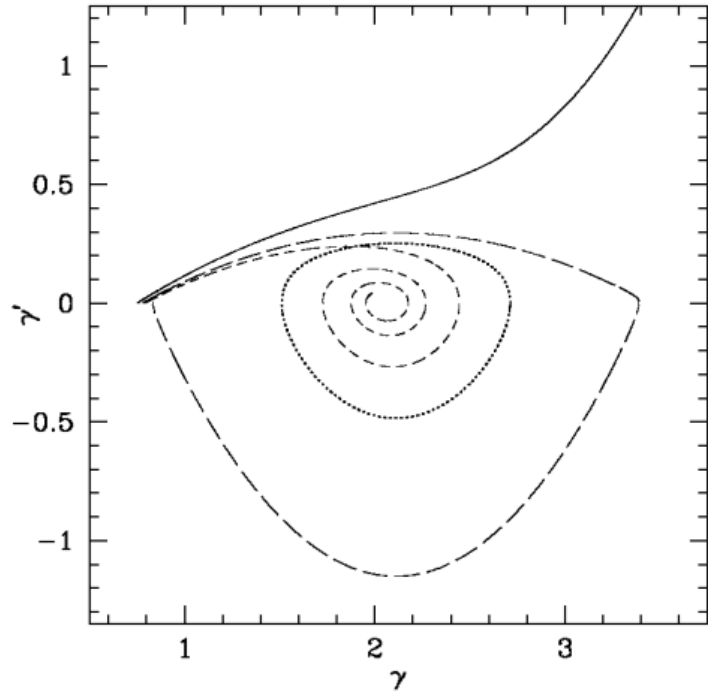


Fig. 11.—  $\gamma'$  vs.  $\gamma$  for a few Jeans equation solutions. ( $\gamma$  is the log-log halo density profile slope.) The solid line approximates the NFW fit. The long-dash line is the limit cycle for equation 5:  $\alpha = 1.9444$ , initial  $\gamma_{in} = (2/5)\alpha + 0.001 = 0.7788$ , initial  $\gamma'_{in} = 0$ . The dotted line (closed loop) also has  $\alpha = 1.9444$ , but different initial  $\gamma_{in} = 2.7111$ , and  $\gamma'_{in} = 0$ . The solid ( $\alpha = 1.875$ ) and short-dash ( $\alpha = 1.975$ ) lines are the same as in Figure 3.4. For both,  $\gamma_{in} = (2/5)\alpha$  and  $\gamma'_{in} \gtrsim 0$ . The top arc (parabola) of the long-dash line has an analytic description, given by equations 7 and 8; the bottom arc (parabola) is described by equations A1 and A2.

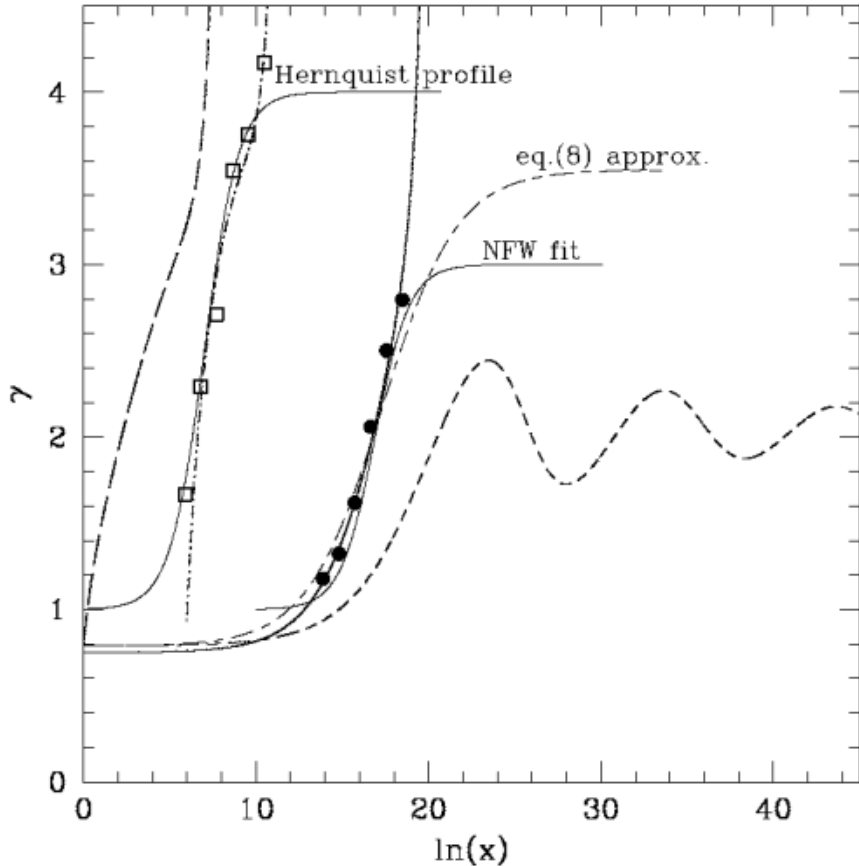


Fig. 12.— Double logarithmic density profile slope,  $\gamma$  vs. radius,  $x$  (arbitrary normalization). The thick solid line is the solution of the Jeans equation that best approximates the NFW fit:  $\alpha = 1.875$ ,  $\gamma'_{in} \gtrsim 0$ . Short-dash ( $\alpha = 1.975$ ,  $\gamma'_{in} \gtrsim 0$ ), long-dash ( $\alpha = 1.975$ ,  $\gamma'_{in} = 1.05$ ) and dot-dash ( $\alpha = 2.27$ ,  $\gamma'_{in} = 2.56$ ) lines are other Jeans equation solutions. All four solutions have  $\gamma_{in} = (2/5)\alpha$ ; see Sections 3.4 and 3.5 for details. The solid and short-dash lines are the same as in Figure 3.4. The empty squares and solid dots represent Models D (Hernquist) and F (NFW) of Kazantzidis et al. (2004). The two thin solid lines are the Hernquist (left) and NFW (right) density profile fits.